Gravure Coating for Roll-to-Roll Manufacturing of Proton-Exchange-Membrane Fuel Cell Catalyst Layers

Scott A. Mauger,[1,z] K. C. Neyerlin,[1] Ami C. Yang-Neyerlin,[2] Karren L. More,[3,*] and Michael Ulsh[1]

[1] *Chemistry and Nanoscience Center, National Renewable Energy Laboratory, Golden, Colorado, USA*
[2] *Department of Chemistry, Colorado School of Mines, Golden, Colorado, USA*
[3] *Center for Nanophase Materials Sciences, Oak Ridge National Laboratory, Oak Ridge, Tennessee, USA*

In this work, we demonstrate gravure coating as a highly relevant technology for the production of roll-to-roll coated catalyst layers. Our results showed gravure coating is capable of coating multi-meter lengths of platinum on carbon catalyst layers at industrially-relevant loadings. Multiple characterization methods were used to examine the microscale and macroscale morphology of the coated layer. Using full-web inspection it was shown that gravure coating produced uniform films in both the cross-web and down-web directions. Using electron microscopy, it was observed that gravure coating produced catalyst layers with larger pores than catalyst layers produced by ultrasonic spray coating. In situ performance testing of the gravure-coated electrodes showed promising results, though additional modifications to the catalyst layer ink and/or drying process are needed to match the catalytic activity of spray-coated catalyst layers. This study lays the foundation for future process science studies to understand the science of scale up.
 [DOI: 10.1149/2.0091813jes]

Manuscript submitted July 5, 2018; revised manuscript received August 29, 2018. Published September 11, 2018.

In recent years Toyota, Honda, and Hyundai have released fuel cell vehicles to consumers. While the current number of vehicles on the road is modest, it is expected to grow substantially in the coming years.[1] With this growth, as well as increased demand from other fuel cell applications (e.g. fork lifts and backup power), there will be a need to quickly translate laboratory-scale technological advances to large-scale manufacturing in order to reduce the price of fuel cell power systems and be cost competitive with other technologies. To meet this demand, understanding the science of scale-up and how the different parameters associated with large-scale processing affect the properties of coated materials and fuel cell performance will be required. Identifying the processing variables that control coated-layer properties and performance is critical for developing robust processes and controls to produce materials that meet specifications. Reliable production of high-performance electrodes will be key to controlling manufacturing costs.

To give a sense of the rates of production that will be needed in the future, a previous analysis estimated that production speeds of 20 m/min of 1 meter wide webs (20 m^2/min) will be needed to produce 15 million fuel cell vehicles per year, which is 10% of the expected 2030 world market.[2] This will require continuous production using roll-to-roll coating methods. Currently, polymer electrolyte membrane fuel cell (PEMFC) components (membranes, diffusion media, and catalyst layers) are and will be produced using roll-to-roll (R2R) coating methods, such as slot-die, gravure, and knife.[3–5] While state-of-the-art membranes and diffusion media used in lab-scale studies are already produced with R2R coating, many state-of-the-art catalyst layers are coated using laboratory techniques such as spray coating (ultrasonic or aerosol) or hand painting to apply the catalyst layer directly to the membrane or the diffusion media. At NREL, ultrasonic spray coating is a reliable and reproducible method for preparing catalyst-coated membrane (CCM) and catalyst coated diffusion media (CCDM) electrodes from 5–400 cm^2.[6,7] We have found that we can ultrasonically spray-coat catalyst layers with state-of-the-art loadings at a rate of about 0.2 m^2/min with one spray nozzle, so with an array of 100 nozzles it might be possible to achieve the required 20 m^2/min speeds noted above.

In practice, most industrial-scale solution processing utilizes coating methods (slot, gravure, slip, etc.) to deposit a liquid film on a substrate at speeds in excess of 10 m/s.[8] The physics and ink formulations are quite different for theses methods than for ultrasonic spray coating. Specifically, ultrasonic spray coating builds up the catalyst layer by coating multiple thin layers over a heated substrate, resulting in rapid drying. Additionally, the catalyst ink is dilute with a typical solid content (catalyst and ionomer) of 0.6 wt%. In contrast, R2R-coated catalyst layers are coated in a single pass using an ink having a much higher solids content of several wt%. This results in differences in coating physics (pressure and shear), drying rate, interparticle interactions, and ink-substrate interactions. As such, the parameters that produce an optimized lab-scale catalyst electrode such as ink formulation (e.g., solvents and solids content), ionomer-to-carbon ratio, or process conditions (e.g., drying temperature) will likely need to be adjusted for R2R-produced catalyst layers to match the performance of lab-scale catalyst layers.

To better understand the necessary adjustments, we have endeavored to understand the materials-process-performance relationships of various PEMFC catalyst layers with the goal of understanding how materials properties and fabrication methodologies relate to fuel cell performance. Over the years, many publications have examined the influence of the solvent on ink properties and fuel cell performance.[9,10] Often the focus was on the solvent dielectric constant and its effect on ionomer conformation in the prepared ink, and the resulting catalyst layer performance. There were also initial reports that examined the influence of leached alloy-catalyst transition metals on ionomer conformation.[11] However, other more process-relevant solvent properties such as vapor pressure have not received as much attention despite the fact that researchers reported a correlation between fuel cell performance and solvent vapor pressure.[12,13] Additionally, there are only limited studies that have examined the evolution of inks throughout the drying and layer formation process.[14] Our overarching goal is to better understand the interplay between material properties (ink formulation, catalyst and support material, substrate), process conditions (coating method, drying rate), and resultant catalyst layer performance. For this work, we focused on determining the coating conditions necessary to create uniform coatings that will enable future studies exploring ink formulation and process conditions in greater detail.

We focused on Pt supported on high surface area carbon (Pt/HSC) catalysts coated onto diffusion media to create CCDM electrodes, sometimes referred to gas diffusion electrodes (GDEs). Diffusion media is an amenable substrate for R2R coating because it does not swell like the membrane, which would make tension control and uniform coating on the R2R web-line difficult. Furthermore, in some circumstances, CCDMs have shown increased high current density performance and lower thermal and high frequency resistances than

*Electrochemical Society Member.
[z]E-mail: scott.mauger@nrel.gov

CCM electrodes, indicating there may be performance benefits for CCDM electrodes.[15]

For this work, we used gravure coating to produce the catalyst layers, as shown in Figure 1a. Gravure coating is a widely used R2R coating method capable of high-uniformity coating of 1–50 μm films at speeds up to 10 m/s (600 m/min), thus it has the capacity for high-volume vehicle production.[16] The gravure method can be used to produce continuous films (coating) or discrete patterns (printing) making it a versatile fabrication method, the latter of which presents an opportunity for high utilization of the Pt catalyst. The diagram in Figure 1b illustrates the fundamentals of gravure coating. An engraved roller known as the gravure cylinder, like that shown in Figure 1c, is rotated through a pan of ink, filling the engraving with the ink. Next a doctor blade is used to remove excess liquid from the gravure cylinder. The flexible web substrate is held in contact with the gravure cylinder through the tension of the system. The ink is transferred to the substrate where the substrate contacts the gravure cylinder, creating the coating. The gravure cylinder can be rotated with (direct) or counter to (reverse) the direction of the substrate. Here we used reverse gravure, where the fluid transfer process is illustrated in Figure 1d. The resulting film thickness is largely determined by the engraved volume of the gravure cylinder, but is also influenced by doctoring, the speed ratio between the gravure cylinder and web, and the fluid properties.[16–18] The volume factor (engraved volume per unit area) is determined by the pattern of the gravure cylinder. While we have used cylinders with a tri-helical pattern in this study, numerous other patterns are available. The disadvantage of gravure coating is that the maximum fluid viscosity and wet film thickness are lower than produced with other techniques, such as slot die.[16,19] These two factors place a more restrictive upper limit on the dry layer thickness; however, we demonstrate that this is not an issue for achieving relevant Pt loadings for commercially viable PEMFC electrodes.

Experimental

The diffusion media used was Sigracet 29BC from SGL Carbon. The rolls were 11 cm by 50 m. The catalyst was 47 wt% Pt/HSC (Tanaka TEC10E50E). The ionomer dispersion was a 20 wt% Nafion (1000 EW) in water and 1-propanol (Nafion D2020, Ion Power). The membrane was a commercially available 25 μm Nafion membrane (NR-211, Ion Power).

The catalyst inks were prepared by weighing the dry catalyst powder into a glass jar, followed by addition of DI water, 1-propanol, and Nafion dispersion, in that order. The weight fraction of catalyst in the ink was 3.2%. The mass ratio of the solvent was 75% 1-propanol/25 wt% water. The ionomer-to-carbon (I:C) mass ratio was either 0.9 or 1.2. Zirconia beads (5 mm) were subsequently added to the jar. The jar was then placed on rollers and the speed was adjusted so that the beads would travel up the side of the jar before tumbling over. The inks were ball milled overnight to disperse the catalyst powder.

Coating was performed on a Mini-Labo Deluxe coating system from Yasui Seki-MIRWEC. Three stainless-steel gravure cylinders (Yasui Seki) with tri-helical patterns of different meshes (lines per inch) were used: 25, 30, and 80, which corresponded to volume factors of 170, 150, and 67 cm^3/m^2, respectively. The diffusion media was conveyed at a linear speed of 1 m/min. with a web tension of approximately 3 lbs. The coatings were dried in a one-meter-long, air–flotation oven at 80°C. The speed of the gravure cylinder was varied between 5 and 35 revolutions per minute, which corresponded to linear speeds of 0.31–2.19 m/min.

Reactive impinging flow (RIF) measurements were performed in a subsequent web-line run following the coating and drying of the catalyst layers to quantify catalyst uniformity. A gas mixture of 2 vol% H_2 and 1 vol% O_2 in N_2 was flowed over the surface of the catalyst layer at 20 standard liters per minute. The web was conveyed at 3.3 feet per min. with a web tension of 0.5 pounds per linear inch. Infrared images were recorded with an infrared thermal camera (Jenoptik) at a rate of 30 frames per second. Each frame was analyzed by measuring the temperature at the same down-web position. The average temperature was calculated for each frame excluding the edges. Further details of the RIF measurement and process can be found in Refs. 20, 21.

Spray-coated CCDM electrodes were prepared using ultrasonic spraying (Sono-Tek). The catalyst powder (4 mg/mL) was mixed with water and 1-propanol (56% v/v water) and Nafion dispersion (0.9 I:C). The inks were dispersed through ultrasonication. First the jar of ink was placed in a beaker filled with ice-water and horn sonicated for 10 s. Next the jar was placed in a bath sonicator filled with ice-water and the ink was sonicated for a total of 20 min. in 5-min. intervals with mild swirling of the ink between intervals. The catalyst ink was sprayed onto the diffusion media, which was heated to 80°C on a temperature-controlled plate. The inks were sprayed at 0.3 mL/min. and a nozzle translational speed of 50 mm/s.

Prior to assembling the membrane electrode assemblies (MEAs), a thin layer of ionomer (approx. 0.045 mg_{Nafion}/cm^2) was ultrasonically spayed on to the catalyst layers from a dilute dispersion of Nafion (2 mg/mL) in water and 1-propanol. This layer of ionomer served to decrease the interfacial resistance between the catalyst layer and the membrane. A detailed explanation of the preparation and function of this layer is forthcoming.

MEAs were prepared by mechanically punching 50 cm^2 of the coated catalyst layers from the rolls. The loadings of the CCDM electrodes were measured using X-ray fluorescence spectroscopy (Fischerscope XDV-SDD, 50 kV, 50 W X-ray source). For each coated section, the loading was measured in at least five locations. The CCDMs and membrane were placed between two 4 inch by 4 inch sheets of Gylon (1/16 inch thick) and 5 inch by 5 inch sheets of Kapton to keep the materials from sticking to the Gylon. This stack was placed between two 1/8 inch thick plates of aluminum. The CCDMs were hot pressed to the membrane for 3 min. at 125°C and 2500 kg of force. The MEAs were allowed to cool to prior to removal from the aluminum plates and separation from the Gylon and Kapton.

For performance testing, the MEAs were assembled into the testing hardware with graphite bipolar plates with triple/double (cathode/anode) serpentine flow fields. The MEAs were sealed between PTFE gaskets and the diffusion media was compressed 25%. The MEAs were pre-conditioned with voltage cycling.[6,7,22] Polarization curves were measured at 80°C, 100%RH, 150 kPa absolute with an anodic sweep direction under voltage control. Oxygen reduction reaction (ORR) mass activity was calculated using high frequency resistance (HRF)-corrected cell potential and H_2-crossover-corrected current. Only current values where the measured current was at least 8x larger than the crossover current were used in this calculation. Three to four MEAs of each type were measured.

Optical microscopy was performed using a Keyence VHX5000 microscope. Images were captured at 200x magnification.

Transmission electron microscopy (TEM) and scanning transmission electron microscopy (STEM) were performed on the gravure-coated and spray-coated catalyst layers. High-resolution TEM and STEM images were acquired from MEA cross-sections using a Hitachi HF3300 TEM/STEM operated at 300 kV. Cross-sections of the electrodes were prepared by embedding in epoxy and slicing ~50–70 nm sections using diamond-knife microtomy (Leica UCT).

Results and Discussion

The following sections detail our findings from gravure coating of Pt/HSC catalyst layers. We report our results on the influence of gravure cylinder volume factor and rotational speed on coating uniformity and loading. The quality of coating was assessed using optical microscopy and RIF measurements and the structure of the coated layers was examined using TEM. Device performance is reported and compared to laboratory-scale, spray-coated catalyst layers.

Gravure coating.—There are two methods of controlling the wet film thickness in gravure coating: engraved volume and cylinder speed. The engraved volume is usually characterized as the volume factor (cell volume per unit surface area) and offers coarse control of the wet film thickness. Varying the cylinder speed offers finer control.

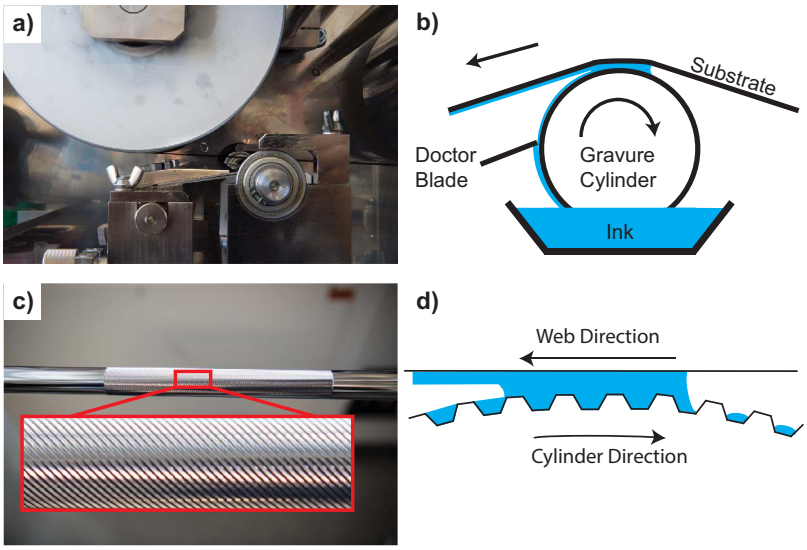

Figure 1. a) Gravure coating station of NREL's R2R coating system. b) Illustration of gravure coating process showing roller rotating through pan of ink. Doctor blade removes excess ink. Remaining ink is then transferred to tensioned web substrate. c) Gravure cylinder with zoom of tri-helical pattern. d) Illustration of fluid transfer process from gravure cylinder to substrate in reverse gravure coating.

The cylinder speed is also important as it influences "pick-out," which is the transfer of fluid from the cells to the substrate. If the cylinder speed or speed ratio (linear speed of cylinder per linear web speed) are not properly tuned it can lead to the formation of defects in the coating.[9,10,16]

As an initial trial, approximately 1-meter lengths of a Pt/HSC catalyst ink (0.9 I:C) were coated with the 25-mesh cylinder (volume factor: 170 cm^3/m^2) at varying speed ratios to understand the influence of this parameter on coating quality and loading. Measurements of the Pt loading and photographs of the coatings for different speed ratios are shown in Figure 2. The plot of loading vs. speed ratio shows that Pt loading increased with increasing speed ratio until it plateaued at speed ratios above 1.5. This trend is consistent with experiments of ink transfer of non-Newtonian fluids in idealized gravure cells

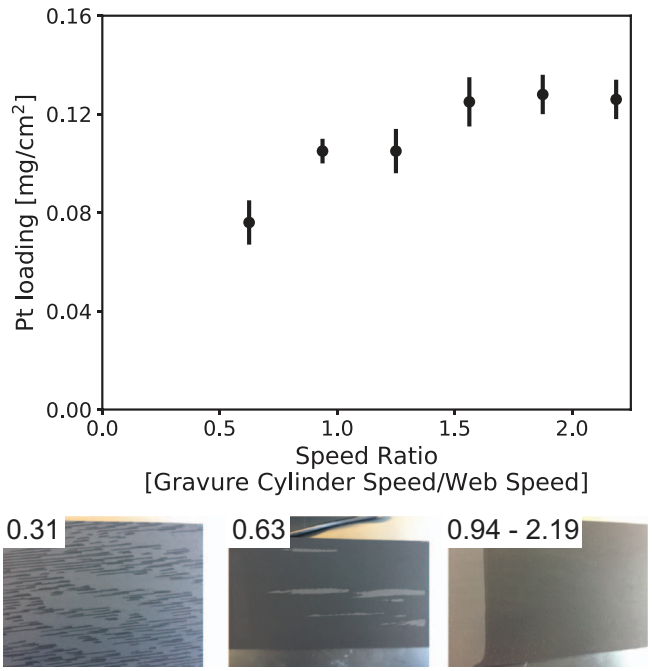

Figure 2. Plot showing gravure-coated catalyst-layer loading as a function of roller speed ratio (top) and photographs of coatings at different roller speed ratios (bottom). Coatings at roller speed ratios above 0.94 were free of visible defects.

that showed the pick-out volume increased with increasing shear or extensional velocity until it reached a plateau.[11,18] It was also observed that low speed ratios lead to poor coating quality. As shown in the bottom of Figure 2, at a roller speed ratio of 0.31 pick-out was poor and only small streaks of catalyst were visible. When the speed ratio was increased to 0.63, the coating quality improved, but large voids were present in the coating. This is known as flashing and is due to incomplete pick-out from the cylinder.[12,13,16,23] Above a speed ratio of 0.94, there were no visible defects in the coatings and we did not observe any pinholes or bubbles. Thus, the range of loadings possible with this ink and cylinder is limited to 0.1–0.13 mg/cm^2. This highlights the limited ability of speed ratio to tune the loading.

Next, the influence of roller volume factor was explored. The 25-mesh cylinder from the previous coating trial was used, as were two cylinders with smaller meshes: 30 (150 cm^3/m^2) and 80 (67 cm^3/m^2). With these cylinders, 1-meter sections of a Pt/HSC ink (1.2 I:C) were coated at three roller speed ratios: 1, 1.5, and 2. These speeds were selected based the previous result that speed ratios above 0.94 were required for consistent coating with the 25-mesh cylinder. As with the previous experiment, we observed that roller speed had a large influence on coating quality but minimal influence on loading. Loading decreased with decreasing volume factor, as expected. Figure 3 shows photographs of the coatings for the different speed ratios with each of the cylinders. We observed that higher speed ratios were required for uniform coatings as the volume factor decreased. For the 80-mesh cylinder (67 cm^2/m^3), even at a roller speed ratio of 2 (upper right of Figure 3), there were still instances of flashing. For these coatings, the Pt loadings (measured in uniformly coated areas) were determined to be ~0.06 mg/cm^2. For the 30-mesh cylinder (150 cm^3/m^2, middle row), flashing was observed at a speed ratio of 1, but uniform (visibly and by Pt loading as measured by XRF) films were obtained at speed ratios of 1.5 and 2. These coatings had loadings ~0.1 mg/cm^2. For the 25-mesh cylinder (170 cm^3/m^2, bottom row) uniform coatings were obtained at all speed ratios, consistent with the previous coating experiment using this cylinder. Additionally, the loadings of the sections coated with the 25-mesh cylinder were ~0.12 mg/cm^2, the same as determined for the previous coating run, demonstrating the reproducibility of gravure coating from run to run.

The observed dependence of coating quality on cylinder mesh and speed ratio is consistent with gravure coating theory. In gravure coating, less than 100% of the fluid volume in the gravure cell is transferred to the substrate. As mentioned previously, the pick-out volume increases with increasing velocity. The pick-out volume also increases with increasing cell width.[14,24] The flashing observed for some combinations of cylinder mesh and speed ratio is explained by these two factors. At low cell widths and low speeds, pick-out is incomplete,

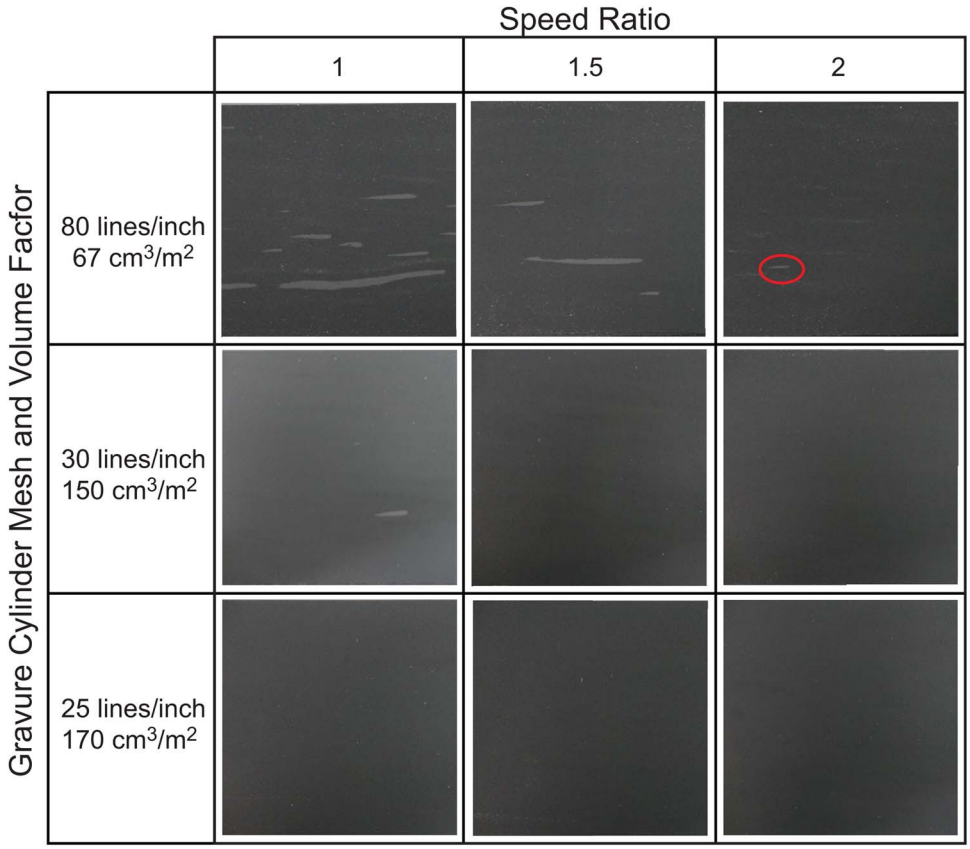

Figure 3. Photographs of gravure-coated catalyst layers as a function of gravure cylinder mesh/volume fraction and speed ratio. All cylinders have same tri-helical-type engraving pattern.

creating voids in the coating. As the cell width and/or speed is increased the pick-out volume increases and flashing is not observed. These results indicate that decreasing the solids concentration (Pt/HSC and Nafion) in the ink may be a better method for decreasing electrode loading than decreasing the cylinder mesh.

Reactive impinging flow characterization.—From the coating experiments, it was clear that varying the process conditions influenced the quality of coating. Macroscale defects were clearly visible to the eye, but more advanced characterization tools were required to discern micro-scale variations in loading. XRF is a useful tool for absolute measurements of loading, however, it is a point measurement technique and thus, full web inspection is not feasible. Additionally, measurements require acquisition times that are too slow to achieve useful resolution in the down-web direction. NREL previously developed a reactive impinging flow (RIF) technique for characterizing the loadings and uniformity of Pt electrodes.[15,20,21] RIF inspection allows full-web characterization of the coating uniformity measured at coating speeds. It has been shown that the thermal response scales with Pt loading.

Figure 4 (top) shows a composite image of the coated material that was analyzed and reported in Figure 2. This image clearly shows the influence of speed ratio on coating uniformity. For the section coated at a 0.63 speed ratio, cold spots due to flashing voids are apparent, consistent with visible observations. The coatings at higher speed ratios are more uniformly colored, indicating uniform coating both cross and down web. Calculation of the average temperature at each down-web length, shown in the lower portion of Figure 4, further illustrates these trends (light blue lines indicate the standard deviations for each position). The deviations for the section coated at 0.63 speed ratio are much larger than those of the coatings at higher speed ratios. These averages also show little down web variation in a given coating section, showing consistent down-web coating uniformity.

The RIF measurements were compared with XRF measurements of the Pt loading. The calculated average temperature and coefficient of variation for each speed-ratio section are compared with the XRF-measured Pt-loading in Table I. The average temperature showed the same trends as the XRF measurements, with higher temperatures corresponding to higher Pt loadings. Additionally, higher temperature variation corresponded with higher loading variation. These results

Table I. Comparison of RIF measured temperature and XRF measured Pt Loading. Average temperature is calculated by taking an average of all points within each speed ratio section excluding edges. Pt loading was measured by XRF at several points from each speed ratio section.

Speed Ratio	Avg. Temp. [°C]	Temp. Coefficient of Variation [%]	Pt Loading [mg/cm^2]	Loading Coefficient of Variation [%]
0.63	61.1	1.2	0.076	11.8
0.94	63.9	0.4	0.105	5.1
1.25	64.6	0.4	0.105	8.2
1.56	64.8	0.3	0.125	8.1
1.88	65.2	0.3	0.128	6.6
2.19	64.5	0.4	0.126	6.0

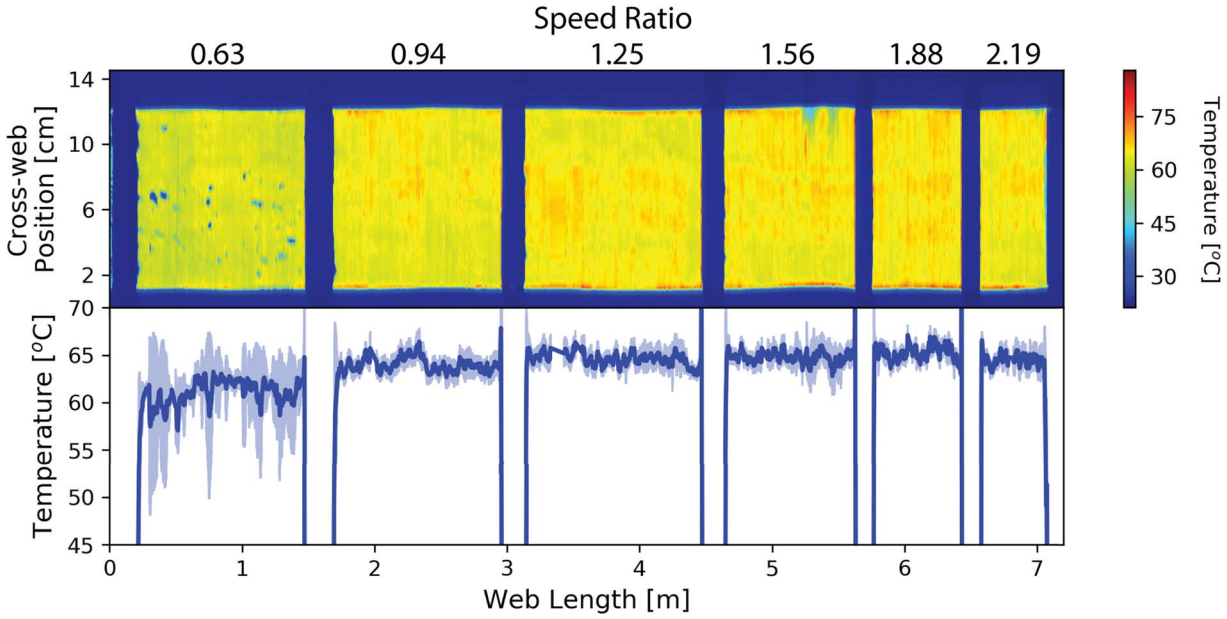

Figure 4. Reactive impinging flow measurements of CCDM roll coated at different roller speed ratios. Top plot shows areal map of the thermal response. Bottom plot shows average temperature (dark blue) with standard deviation (light blue) as a function of web length.

clearly showed that gravure coating is capable of coating uniform catalyst layers at technically relevant loadings.

Microscopy.—Visual and RIF inspection of the coatings provided information about macroscale defects, but are not able to identify defects and features at the micro- and nanoscale. Optical microscopy was used to study the quality of the coatings. Figure 5 shows images of (a) an uncoated microporous layer (MPL), (b) a gravure-coated catalyst layer, and (c) a spray-coated catalyst layer. The uncoated MPL was very rough with many cracks. For the gravure-coated catalyst layer, the majority of the MPL cracks did not extend into the catalyst layer coating, aside from a few spots where small holes were observed in the film. The inks used for gravure coating were viscous and shear thinning. Once the applied stress of the coating process is removed, the inks will thicken, preventing them from flowing into the MPL cracks during the drying process. Another important observation was that the coating process did not create any air bubbles or other microscale coating defects. In contrast, the MPL cracks persisted for a spray-coated catalyst layer. The spray-coating ink was dilute and Newtonian, so it flowed easily into the cracks. Several reports studied the effects of cracks in fuel cell materials.[16–18,25–29] In CCM MEAs, cracks in the MPL have been shown to improve initial fuel cell performance,[26] while catalyst layer cracks induce membrane failure.[29] The implications of catalyst layer cracks in CCDMs have not been reported. Thus, it is unknown whether or not reduction in cracks from gravure coating will be benficial.

TEM and high-angle annular dark field scanning transmission electron microscopy (HAADF-STEM) were used to study the nanoscale structure of these catalyst layers. The TEM (top row) and HAADF-STEM (bottom row) images shown in Figure 6 compare Pt/HSC catalyst layers (0.9 I:C) coated via (a,c) gravure and (b,d) spray methods. From the TEM images in (a) and (b), it was observed that the Pt nanoparticle size did not differ between the two coating methodologies. The most noticeable difference between the two coating methods was the difference in catalyst layer pore size (shown with red outlines). The gravure-coated electrode had significantly larger pores than the spray-coated electrode, indicating a less dense electrode structure.

Another significant observation was the cross-sectional HAADF-STEM images (b,d) showed no significant penetration of catalyst into the MPL, regardless of coating method used. Simulations and experiments have shown that a slot-coated non-Newtonian fluid (similar to the catalyst ink used here) will significantly penetrate into porous carbon paper.[30] However, we do not believe that this difference is due to the coating method used, but is due to the diffusion media used in the present experiments having an MPL. Ding, et al., coated onto Toray paper without an MPL.[24] The smaller pores of the MPL likely prevented significant penetration of the catalyst into the diffusion media.

The cross-sectional HAADF-STEM images (Figures 6c, 6d) showed the gravure-coated layers were less dense than the spray-coated layers, consistent with the pore sizes (red outlines) observed in the TEM images (Figures 6a, 6b). The thickness of the gravure-coated catalyst layer is relatively uniform, even at the micro-scale. In

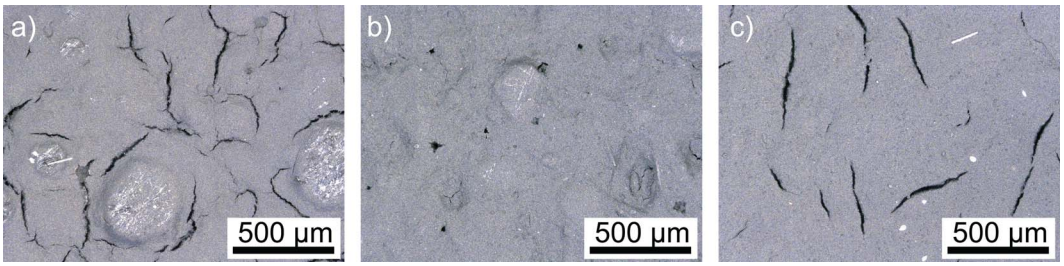

Figure 5. Optical images of a) MPL of uncoated SGL 29BC, b) gravure coated catalyst layer on SGL 29BC, and c) ultrasonic spray-coated catalyst layer on SGL 29BC.

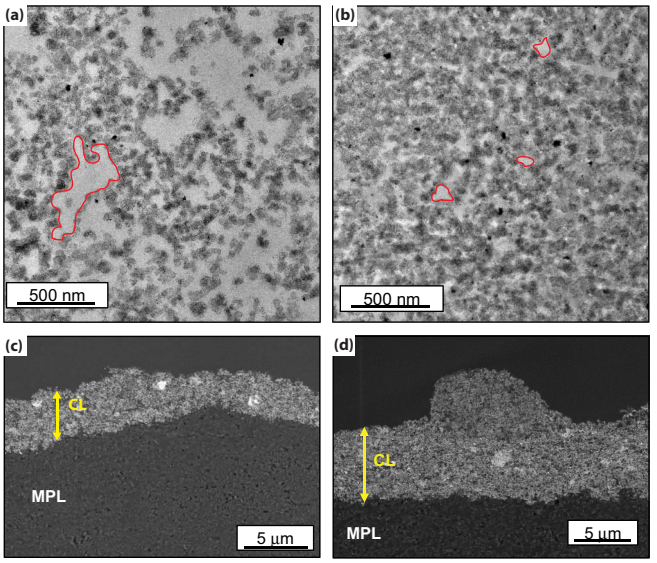

Figure 6. TEM images of (a) gravure-coated and (b) spray-coated catalyst layers. The red lines highlight secondary pores in the catalyst layers. Cross-sectional high-angle annular dark field (HAADF)-STEM images of (c) gravure-coated and (d) spray-coated CCDMs. Difference in catalyst layer thickness is due to differences in loading between gravure and spray coated layers. Gas diffusion layer beneath MPL is not shown.

contrast, the spray-coated catalyst layer shows significant variations in thickness. This could be due to the inefficiencies in the ultrasonic spray coating process, which may not always properly breakup the ink into fine droplets. Additionally, both coatings exhibited relatively large Pt/HSC agglomerates ~1 µm (visible in HAADF-STEM images as large bright spots - Figures 6c, 6d).

There are two possible explanations for the different porosity observed for the two coating methods, which relate to our goal of understanding materials-process-performance relationships. The first explanation is the coating method used. During spray coating, the layer is built-up by multiple passes of the spray nozzle, with each pass depositing roughly 0.01 mg_{Pt}/cm^2.[31] Any large voids or pores created during a single pass could be filled by the subsequent pass, leading to a denser film. Also, each new pass could dissolve some of the dried catalyst allowing it another chance to rearrange and pack more densely. In contrast, with gravure coating the catalyst layer is coated in a single pass and dried in an oven. The drying of thick liquid films, like those produced by gravure coating in this study, tend to be evaporation dominated, as opposed to diffusion or sedimentation dominated.[32] In evaporation-dominated drying, solid particles collect at the liquid-air interface as the liquid is evaporated. If the time scale for particles arriving at this interface is shorther than that of reorganization, there is not sufficient time for the particles to pack closely together, resulting in a more disordered packing. Such disordered packing would lead to the larger pores that we observed in our gravure-coated catalyst layers. Decreasing the concentration of particles, like in the spray-coated inks, increases the sedimentation and diffusion rates, the latter making it more likely that particles will be able to rearrange into a more densely packed structure.

The second explanation is differences in the concentration of the catalyst inks. Carbon black dispersions form fractal networks, which above a critical concentration will transition from a liquid to a gel with a stress bearing network that spans the volume of the suspension.[33] Ultra-small angle X-ray scattering studies have shown that these extended fractal networks are also present in the catalyst inks.[34] The inks used for spray coating were very dilute, with 0.6 wt% total solids; thus the Pt/HSC agglomerates will be small and can pack closely together during the drying process. In contrast, the inks used for gravure coating were almost an order of magnitude more concentrated than the spray coating ink leading to much larger Pt/HSC catalyst agglomerates. TEM images show that these large agglomerates are irregularly shaped.[34] Larger Pt/HSC agglomerates combined with the increased viscosity of the concentrated ink could inhibit close packing of the catalyst, thereby resulting in a more porous structure.

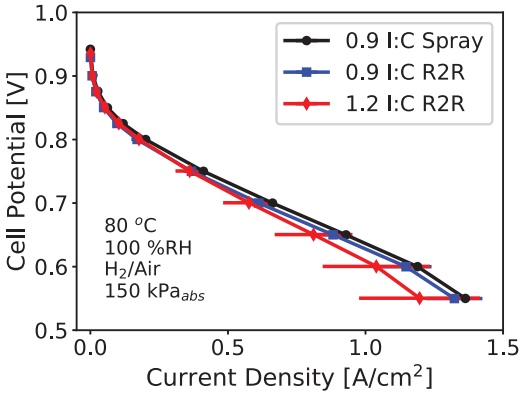

Figure 7. Average H_2/air polarization curves measured at 80°C and 100%RH for MEAs with R2R-coated and spray-coated CCDM electrodes. Cathode loadings were 0.1–0.12 mg_{Pt}/cm^2. Membrane was 25 µm Nafion for all MEAs.

MEA performance.—MEAs were prepared from gravure-coated catalyst layers coated from inks with 0.9 and 1.2 I:C ratios, and spray-coated catalyst layers with 0.9 I:C ratio. For spray-coated catalyst layers with a HSC support, an I:C of 0.9 is reported to be the optimized value based on the support surface area and the influence of I:C on the catalyst layer proton resistance and cell performance.[35] The electrodes were hot pressed onto 25 µm thick Nafion membranes. All cathodes had Pt loadings of 0.1–0.12 mg/cm^2. In order to achieve high performance, all CCDM electrodes were coated with a thin layer of spray-coated ionomer. While the exact function of this ionomer layer will be detailed in a subsequent publication, in general, the presence of such an ionomer layer lowers interfacial resistance between the membrane and electrode, improving both mass activity and high current density performance. Average H_2/air polarization curves for multiple MEAs are shown Figure 7. The average ORR mass activity at 0.9 V (150 kPa, 100%RH, 80°C H_2/O_2, HFR- and H_2 crossover corrected) and current density at 0.6 V (150 kPa, 100%RH, 80°C H_2/Air) are shown in Table II. The gravure-coated CCDM MEAs had moderately lower mass activity values than the spray-coated CCDM MEAs. Interestingly, for the gravure-coated MEAs, a 0.9 I:C ratio, which is the optimal I:C ratio for spray-coated catalyst layers, resulted in slightly lower mass activity than a 1.2 I:C ratio.

In contrast with mass activity, 1.2 I:C resulted in slightly inferior high current density performance, as indicated by the measured current density at 0.6 V. Despite the lower mass activity of the 0.9 I:C gravure-coated CCDM MEAs, these MEAs had comparable high current density performance to the spray-coated CCDM MEAs. Given the deviation in these measured values, it is hard to conclusively state that the differences are meaningful. It is possible that the higher ionomer

Table II. Average performance metrics for spray-coated and gravure-coated CCDM MEAs. ORR mass activities ($i_m^{0.9V}$) calculated (HFR- and H_2-crossover corrected) from H_2/O_2 polarization curves measured in an anodic sweep direction. H_2/Air and H_2/O_2 polarization curves measured at 80°C, 100%RH, and 150 kPa_{abs}.

Coating Method	I:C	$i_m^{0.9V}$ (mA/mg_{Pt})	$i^{0.6V}$ (A/cm^2)
Spray	0.9	372 ± 13	1.18 ± 0.01
Gravure	0.9	296 ± 21	1.15 ± 0.11
Gravure	1.2	322 ± 38	1.04 ± 0.22

content may be limiting mass transport in the catalyst layer by reducing the porosity or creating a thicker ionomer film covering the catalyst.

These results suggest that the optimal I:C ratio may be different for R2R-coated catalyst layers than spray-coated catalyst layers. Ultrasonic spraying produces a discrete ionomer layer with each subsequent pass while the ionomer distribution within the gravure-coated catalyst layer is subject to the effects of solvents and drying conditions; thus, it is not necessarily surprising that the optimum I:C ratios for the two processes could different.

There are numerous potential explanations (coating method, ink dispersion method, ink formulation, etc.) for the differences observed in performance between the gravure-coated and spray-coated CCDM MEAs. These process differences will need to be investigated in greater detail to determine their influence on catalyst layer properties and MEA performance and will be the subject of future studies.

Conclusions

The results demonstrated gravure-coating as a viable methodology for coating uniform PEMFC catalyst layers at technologically relevant loadings. We found that gravure cylinder volume factor provided coarse control of catalyst layer loading, while the speed ratio offered finer control. We also found that larger gravure cylinder volume factors resulted in uniform films for a wider range of speed ratios than cylinders with lower volume factors. Differences in morphology and performance were observed between gravure-coated and spray-coated electrodes. Gravure-coated catalyst layers exhibited a more uniform thickness and larger pore sizes than spray-coated catalyst layers. Gravure-coated electrodes had lower ORR mass activities than spray-coated electrodes but had similar high current density performance. These performance results demonstrate the need for additional studies on roll-coated catalyst layers to understand how inks should be formulated and processed to achieve similar performance to high-performance, laboratory-scale catalyst layers. Understanding this and other materials-process-performance relationships is critical to reducing the time and trial-and-error involved in transitioning promising new materials from the laboratory to large-scale production for fuel cells and other electrochemical energy conversion technologies.

Acknowledgments

This work was authored in part by the National Renewable Energy Laboratory, operated by Alliance for Sustainable Energy, LLC, for the U.S. Department of Energy (DOE) under Contract No. DE-AC36-08GO28308. Funding provided by U.S. Department of Energy, Office of Energy Efficiency and Renewable Energy, Fuel Cell Technologies Office, program manager Nancy Garland. Microscopy performed as part of a user project at ORNL's Center for Nanophase Materials Sciences, which is a U.S. Department of Energy, Office of Science User Facility. The views expressed in the article do not necessarily represent the views of the DOE or the U.S. Government. The U.S. Government retains and the publisher, by accepting the article for publication, acknowledges that the U.S. Government retains a nonexclusive, paid-up, irrevocable, worldwide license to publish or reproduce the published form of this work, or allow others to do so, for U.S. Government purposes.

ORCID

Scott A. Mauger https://orcid.org/0000-0003-2787-5029
Karren L. More https://orcid.org/0000-0001-5223-9097

References

1. California Environmental Protection Agency Air Resources Board, 2017 Annual Evaluation of Fuel Cell Electric Vehicle Deployment and Hydrogen Fuel Station Network Development, (2017).
2. M. K. Debe, "Electrocatalyst approaches and challenges for automotive fuel cells," *Nature*. **486**, 43 (2012).
3. T. Steenberg, H. A. Hjuler, C. Terkelsen, M. T. R. Sánchez, L. N. Cleemann, and F. C. Krebs, "Roll-to-roll coated PBI membranes for high temperature PEM fuel cells," *Energy Environ. Sci.*, **5**, 6076 (2012).
4. R. Baumann, A. Willert, F. Siegel, and A. Kohl, Method for producing catalyst layers for fuel cells, U. S. Pat. Office. (2012).
5. M. Stähler and I. Friedrich, "Statistical investigations of basis weight and thickness distribution of continuously produced fuel cell electrodes," *J. Power Sources.*, (2013).
6. S. A. Mauger, K. C. Neyerlin, S. M. Alia, C. Ngo, S. Komini Babu, K. E. Hurst et al., "Fuel Cell Performance Implications of Membrane Electrode Assembly Fabrication with Platinum-Nickel Nanowire Catalysts," *J. Electrochem Soc*. **165**, F238 (2018).
7. K. C. Neyerlin, J. M. Christ, J. W. Zack, W. Gu, S. Kumaraguru, A. Kongkanand et al., "New Insights from Electrochemical Diagnostics Pertaining to the High Current Density Performance of Pt-Based Catalysts," *230th ECS Meeting*. MA2016-02, 2492 (2016).
8. S. F. Kistler and P. M. Schweizer, eds., *Liquid Film Coating*, Chapmap and Hall, 1997.
9. S. Shukla, S. Bhattacharjee, A. Z. weber, and M. Secanell, "Experimental and Theoretical Analysis of Ink Dispersion Stability for Polymer Electrolyte Fuel Cell Applications," *J. Electrochem. Soc.*, **164**, F600 (2017).
10. M. Shibayama, T. Matsunaga, T. Kusano, K. Amemiya, N. Kobayashi, and T. Yoshida, "SANS studies on catalyst ink of fuel cell," *J. Appl. Polym. Sci.*, **131**, 39842 (2014).
11. D. Myers, Rationally Designed Catalyst Layers for PEMFC Performance Optimization, *2016 DOE Hydrogen and Fuel Cell Program Review*. (2016).
12. T.-H. Yang, Y.-G. Yoon, G.-G. Park, W.-Y. Lee, and C.-S. Kim, "Fabrication of a thin catalyst layer using organic solvents," *J. Power Sources.*, **127**, 230 (2004).
13. R. Fernández, P. Ferreira-Aparicio, and L. Daza, "PEMFC electrode preparation: Influence of the solvent composition and evaporation rate on the catalytic layer microstructure," *J. Power Sources.*, **151**, 18 (2005).
14. T. Kusano, T. Hiroi, K. Amemiya, M. Ando, T. Takahashi, and M. Shibayama, "Structural evolution of a catalyst ink for fuel cells during the drying process investigated by CV-SANS," *Polym J*. **47**, 546 (2015).
15. D. W. Fultz and P.-Y. A. Chuang, "The Property and Performance Differences Between Catalyst Coated Membrane and Catalyst Coated Diffusion Media," *Journal of Fuel Cell Science and Technology*. **8**, 041010 (2011).
16. F. R. Pranchk and D. J. Coyle, *Elastohydrodynamic Coating Systems*, in: S. F. Kistler and P. M. Schweizer, (Eds.), Liquid Film Coating, Chapman and Hall, 1997.
17. S. Khandavalli, J. A. Lee, M. Pasquali, and J. P. Rothstein, "The effect of shear-thickening on liquid transfer from an idealized gravure cell," *J. Nonnewton. Fluid Mech.*, **221**, 55 (2015).
18. S. Khandavalli and J. P. Rothstein, "Ink transfer of non-Newtonian fluids from an idealized gravure cell: The effect of shear and extensional deformation," *J. Nonnewton. Fluid Mech.*, **243**, 16 (2017).
19. X. Ding, J. Liu, and T. A. L. Harris, "A review of the operating limits in slot die coating processes," *AIChE J*. **62**, 2508 (2016).
20. M. Ulsh, J. M. Porter, D. C. Bittinat, and G. Bender, "Defect Detection in Fuel Cell Gas Diffusion Electrodes Using Infrared Thermography," *Fuel Cells*. **16**, 170 (2016).
21. I. V. Zenyuk, N. Englund, G. Bender, A. Z. Weber, and M. Ulsh, "Reactive impinging-flow technique for polymer-electrolyte-fuel-cell electrode-defect detection," *J. Power Sources.*, **332**, 372 (2016).
22. P. A. Rapaport, A. J. Blowers, L. James, and B. Lakshmanan, Fast MEA break-in and voltage recovery, U. S. Pat. Office. 9099703 (2015).
23. E. B. Gutoff and E. D. Cohen, *Coating and Drying Defects*, John Wiley & Sons, 2006.
24. D. M. Campana and M. S. Carvalho, "Liquid transfer from single cavities to rotating rolls," *J. Fluid Mech.*, **747**, 545 (2014).
25. S. M. Kim, C.-Y. Ahn, Y.-H. Cho, S. Kim, W. Hwang, S. Jang et al., "High-performance Fuel Cell with Stretched Catalyst-Coated Membrane: One-step Formation of Cracked Electrode," *Sci. Rep.*, **6**, 48 (2016).
26. I. V. Zenyuk, R. Taspinar, A. R. Kalidindi, E. C. Kumbur, and S. Litster, "Computational and Experimental Analysis of Water Transport at Component Interfaces in Polymer Electrolyte Fuel Cells," *J. Electrochem. Soc.*, **161**, F3091 (2014).
27. Y. Singh, F. P. Orfino, M. Dutta, and E. Kjeang, "3D Failure Analysis of Pure Mechanical and Pure Chemical Degradation in Fuel Cell Membranes," *J. Electrochem. Soc.*, **164**, F1331 (2017).
28. S. Kundu, M. W. Fowler, L. C. Simon, and S. Grot, "Morphological features (defects) in fuel cell membrane electrode assemblies," *J. Power Sources.*, **157**, 650 (2006).
29. M. Pestrak, Y. Li, S. W. Case, D. A. Dillard, M. W. Ellis, Y.-H. Lai et al., "The Effect of Mechanical Fatigue on the Lifetimes of Membrane Electrode Assemblies," *Journal of Fuel Cell Science and Technology*. **7**, 041009 (2010).
30. X. Ding, T. F. Fuller, and T. A. L. Harris, "Predicting fluid penetration during slot die coating onto porous substrates," *Chem. Eng. Sci.*, **99**, 67 (2013).
31. M. B. Sassin, Y. Garsany, B. D. Gould, and K. E. Swider-Lyons, Fabrication Method for Laboratory-Scale High-Performance Membrane Electrode Assemblies for Fuel Cells, *Anal. Chem.*, **89**, 511 (2016).
32. C. M. Cardinal, Y. D. Jung, K. H. Ahn, and L. F. Francis, "Drying regime maps for particulate coatings," *AIChE J*. **56**, 2769 (2010).
33. J. J. Richards, J. B. Hipp, J. K. Riley, N. J. Wagner, and P. D. Butler, "Clustering and Percolation in Suspensions of Carbon Black," *Langmuir*. (2017).
34. F. Xu, H. Zhang, J. Ilavsky, L. Stanciu, D. Ho, M. J. Justice et al., "Investigation of a Catalyst Ink Dispersion Using Both Ultra-Small-Angle X-ray Scattering and Cryogenic TEM," *Langmuir*. **26**, 19199 (2010).
35. Y. Liu, C. Ji, W. Gu, J. Jorne, and H. A. Gasteiger, "Effects of Catalyst Carbon Support on Proton Conduction and Cathode Performance in PEM Fuel Cells," *J. Electrochem. Soc.*, **158**, B614 (2011).